Epidemie e stagionalità

Prof. Sergio Ortolani
Dipartimento di Fisica e Astronomia, Università di Padova

Epidemic, coronavirus (COVID) seasonality

(Martinez, M., 2018; Kronfed-Schor et al., 2021; Cohen, J., Science, 2020)

"If we knew what suppressed influenza to summertime levels, that would be a lot more effective than any of the flu vaccines we have."

Scott Dowell, Bill & Melinda Gates Foundation

Environment seasonal drivers:
(1) transmission,
(2) host conditions and behaviour,
(3) nonhuman host (**Martinez, 2018**)

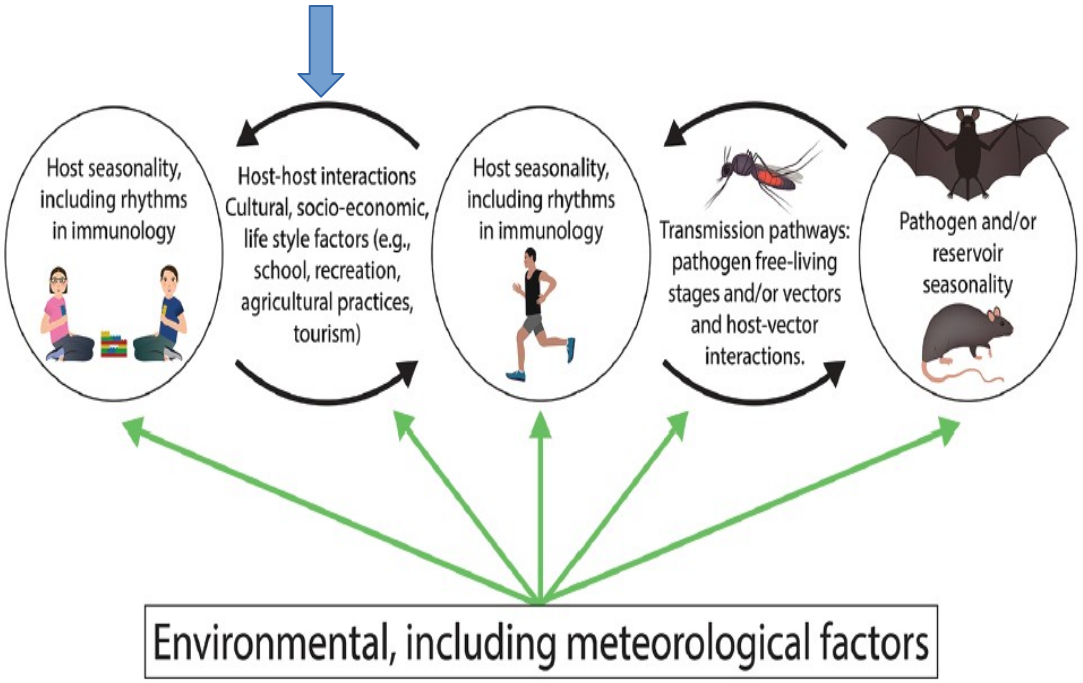

Figure 1. Candidate drivers of disease seasonality. Circles show organisms implicated in disease transmission, black arrows indicate their interactions, and green arrows indicate the influence of environmental factors.

The calendar of epidemics

At least 68 infectious diseases are seasonal, according to a 2018 paper by Micaela Martinez of Columbia University. But they're not in sync, and seasonality varies by location. Here, each bubble represents the percentage of annual cases that occurred in each month. (The data are old because many diseases declined—in some cases to zero—after the introduction of vaccines.)

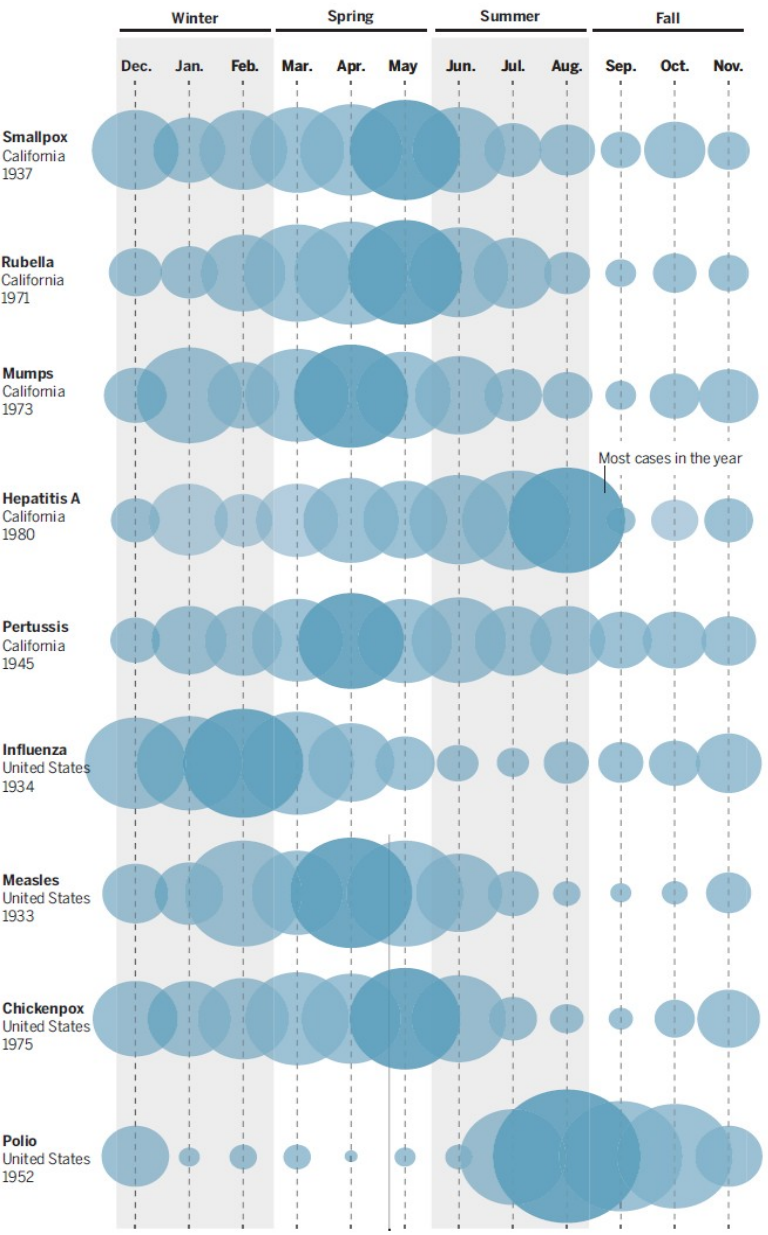

PEARLS

The calendar of epidemics: Seasonal cycles of infectious diseases

Micaela Elvira Martinez *

Climate & Health, Department of Environmental Health Sciences, Mailman School of Public Health, Columbia University, New York, New York, United States of America

* mem2352@cumc.columbia.edu

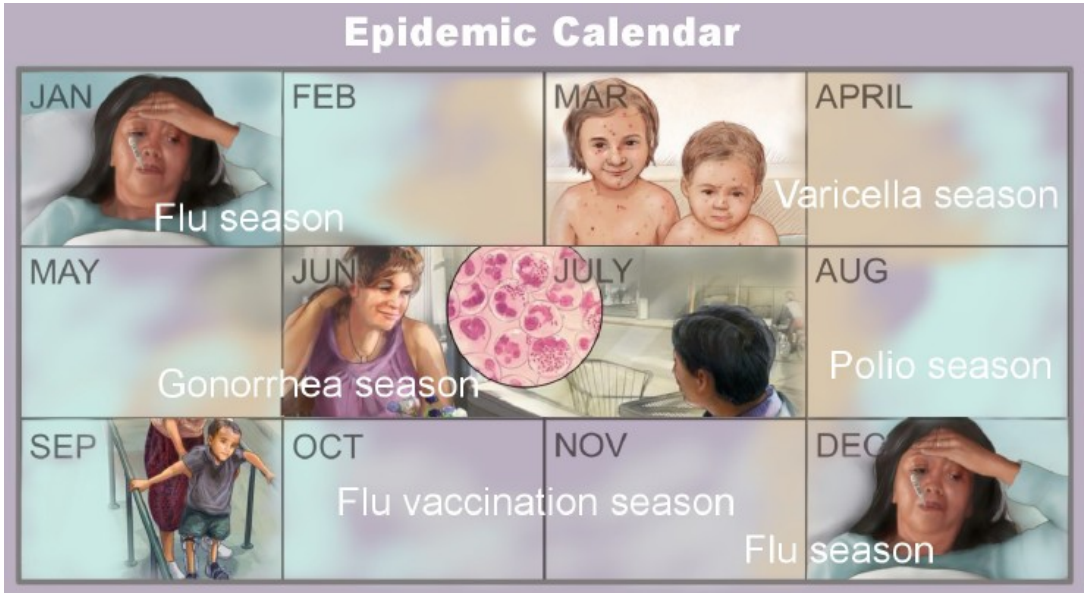

Seasonality of **coronaviruses** (Kronfeld-Schor et al., 2021): winter-spring peaks

Very low autumn !

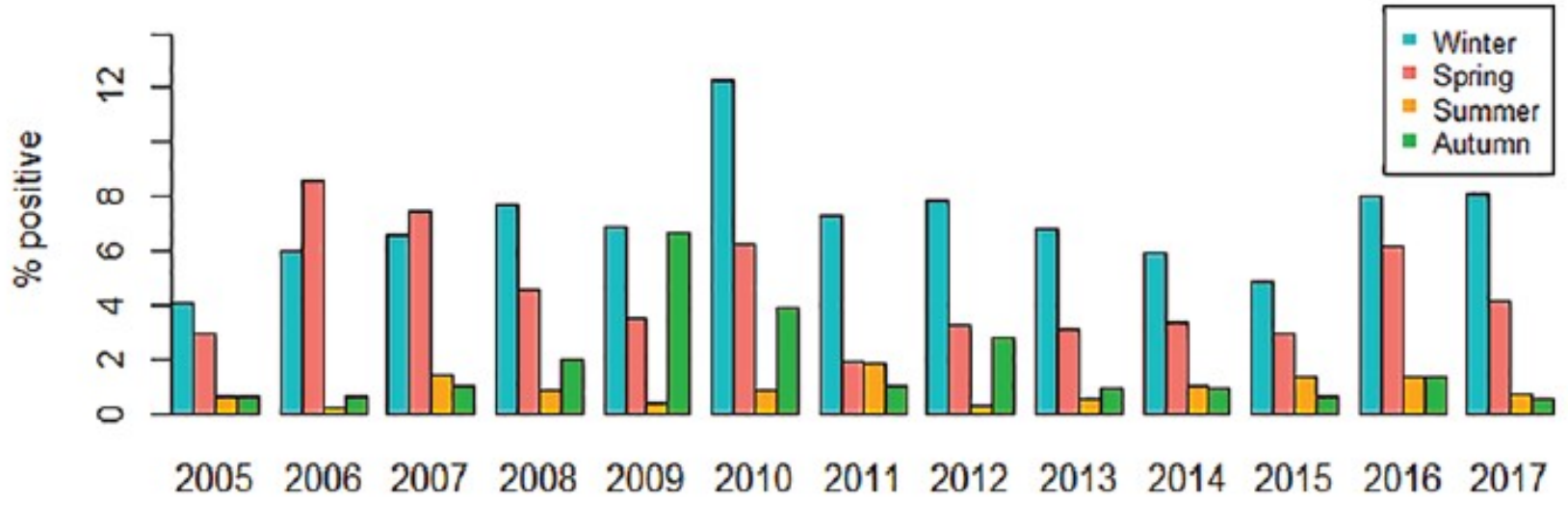

Figure 2. Seasonality of endemic human coronaviruses (CoV-OC43, CoV-NL63, and CoV-229E species) detected in a large urban patient population. The percentage (%) of human coro-

Shaman J, Kohn M. Absolute Humidity Modulates Influenza Survival, Transmission, and Seasonality. Proceedings of the National Academy of Sciences of the United States of America. 2009; 106 (9):3243–8. https://doi.org/10.1073/pnas.0806852106 PMID: 19204283

ESC European Society of Cardiology
Cardiovascular Research
doi:10.1093/cvr/cvaa288

COVID-19: Absolute humidity or dust pollution, or… temperature ???
Or UV !

Regional and global contributions of air pollution to risk of death from COVID-19

Andrea Pozzer [1,2], Francesca Dominici[3], Andy Haines[4], Christian Witt [5], Thomas Münzel [6,7]*, and Jos Lelieveld [2,8]*

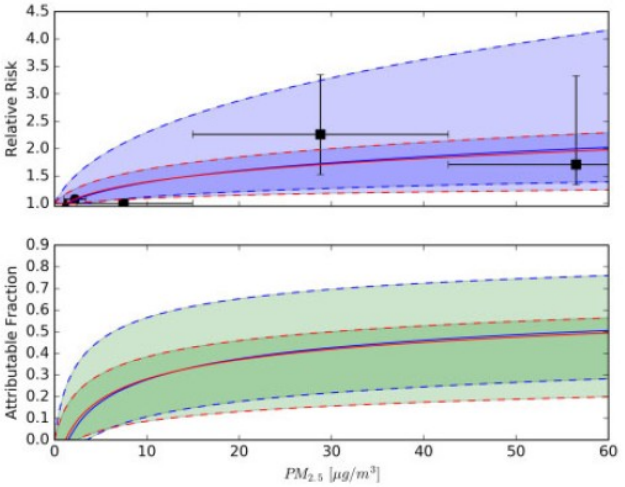

Figure 1 Exposure-response dependencies, based on a log-normal relationship[28]. The relative risk (or hazard ratio), from which the attributable fraction has been derived, is based on mortality rate ratios attributed to air pollution in the COVID-19 pandemic[7] and the SARS epidemic[17], indicated by the black bullet and squares, respectively. The triangle represents the threshold concentration below which $PM_{2.5}$does not have health implications[2]. The red curves depict the function fitted to the data from COVID-19 in the USA only[7], plus the threshold[2] (triangle and bullet). The blue curves depict the function fitted to all data[2,7,17]. The colored ranges show the 95% confidence intervals, which are wider after including the SARS-related results (blue), mostly due to uncertainty from converting Chinese API's into $PM_{2.5}$concentrations (black squares).

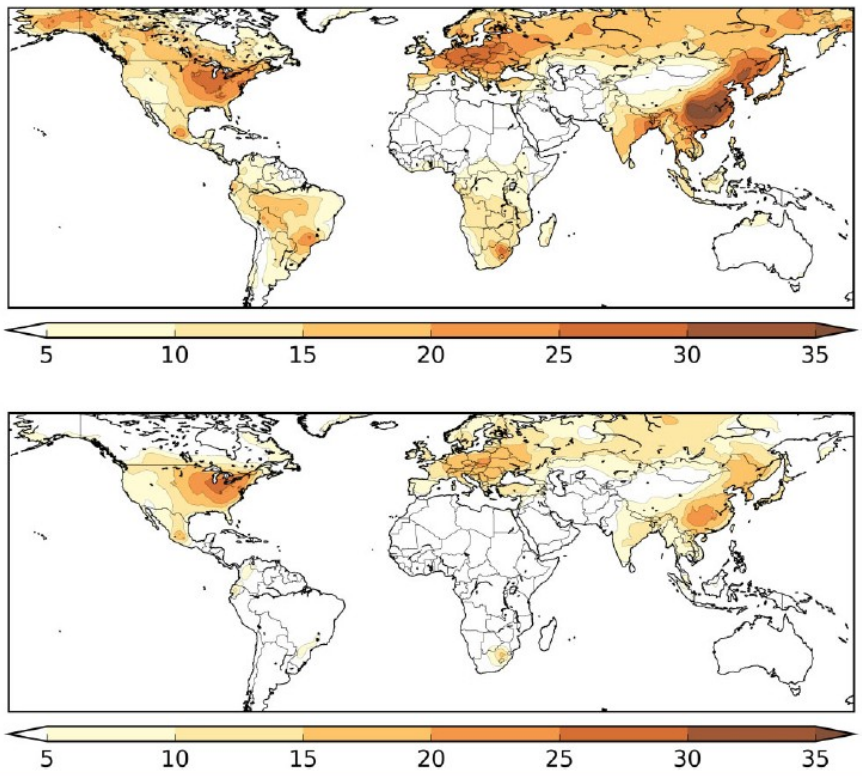

Figure 2 Estimated percentages of COVID-19 mortality attributed to air pollution from all anthropogenic sources (top), and from fossil fuel use only (bottom). The regions with high attributable fractions coincide with high levels of air pollution. The mapped results account for population density, thus reflecting population weighted exposure to PM$_{2.5}$

Rapporto annuale ARPAV 2019. Stagionalità PM10: ruolo del riscaldamento domestico. Taglio netto 15/3 e 15/10.
Curva simmetrica
RADIAZIONE UV ? → Estinzione atmosferica in UV

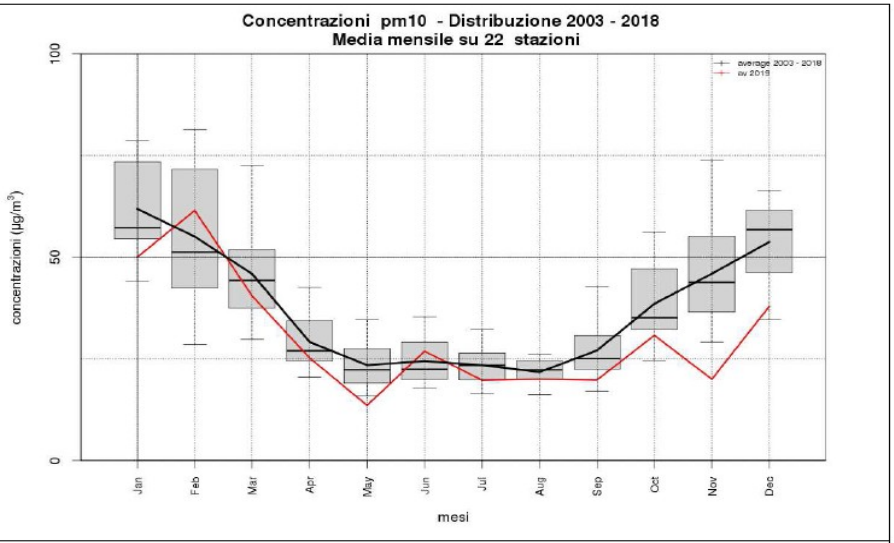

Figura 39: concentrazioni, medie mensili, di PM10 delle stazioni di qualità dell'aria di ARPA Veneto per l'anno 2019 (linea rossa) e media degli anni 2003-2018 (linea nera). L'andamento medio mensile degli anni dal 2003 al 2018 è rappresentato anche mediante box and whiskers plot. Per l'interpretazione del box and whiskers plot fare riferimento alla **Tabella 9** Come interpretare il box and whiskers .

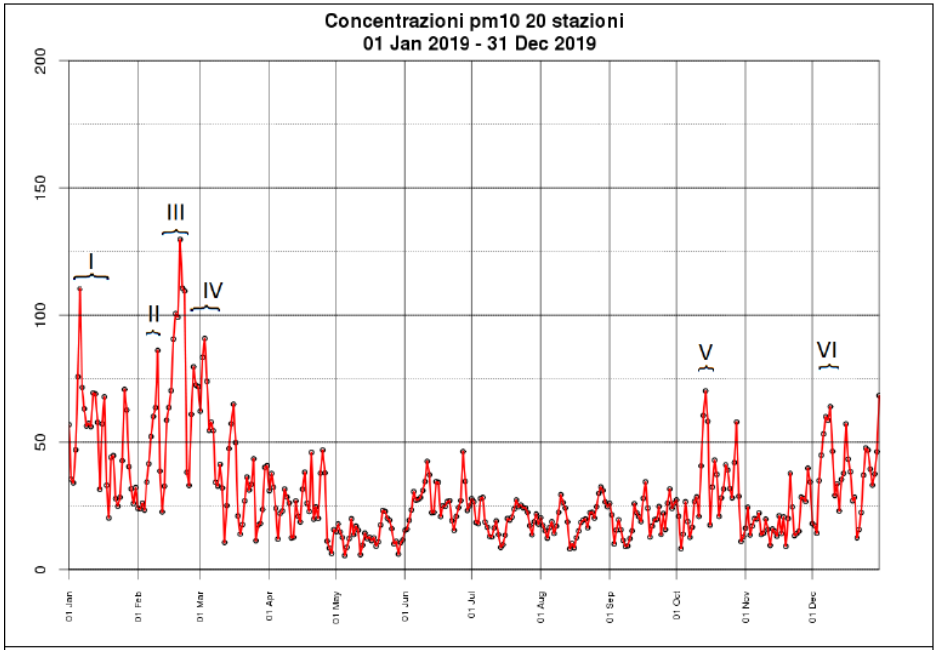

Figura 45: Andamento della media giornaliera delle concentrazioni di PM10, calcolata a partire dai dati delle stazioni di qualità dell'aria automatiche di pianura inserite nel piano di valutazione, riferita all'anno 2019.

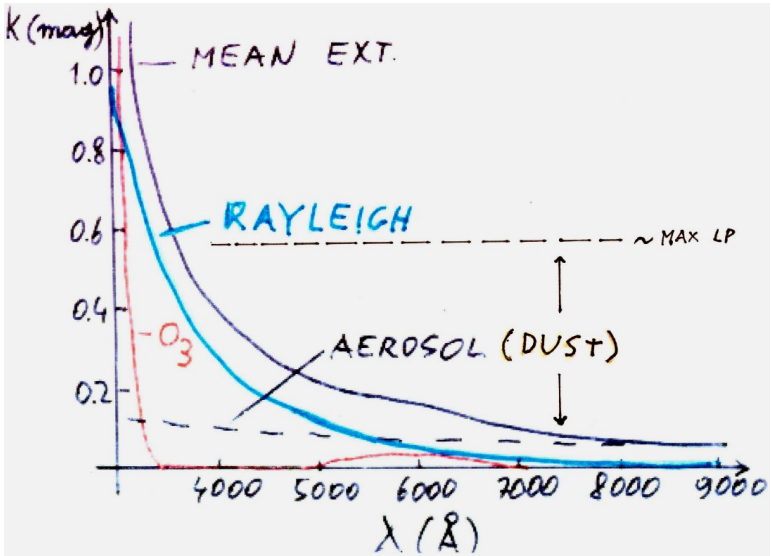

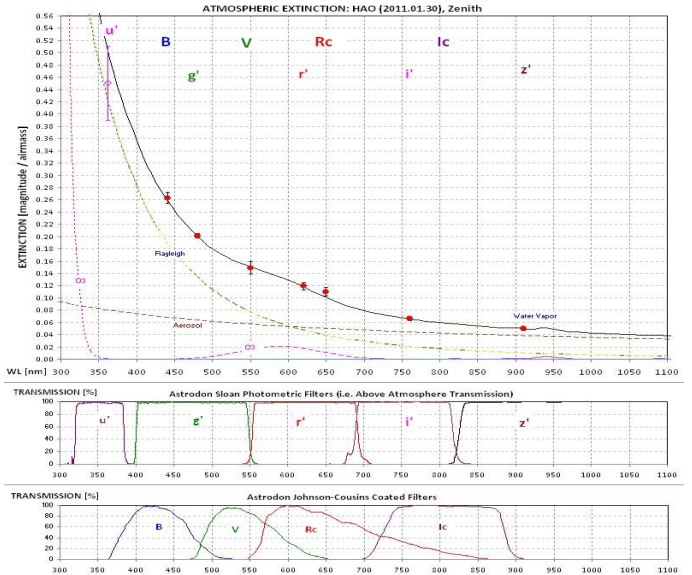

Misure di ozono: ozono stratosferico (TOMS) e troposferico (locale)

OZONO: serie temporali, attività solare, vulcani, *total ozone* e *effective ozone*, massa d'aria, buco dell'ozono

Elio Antonello - Versione 1: 16.7.2020; 2: 21.8.2020

TOMS: polar satellites at noon, res. 30-110 km.

Measurements down to about 1500m above sea level

Nimbus 7 (1978-1994)

Meteor 3 (1991-1994)

Earth Probe (1996-2006)

OMI, SUOMI etc. (2006 ->)

Spessore ozono stratosferico, Italia, Torino durante l'anno. Unità Dobson (mmx100)

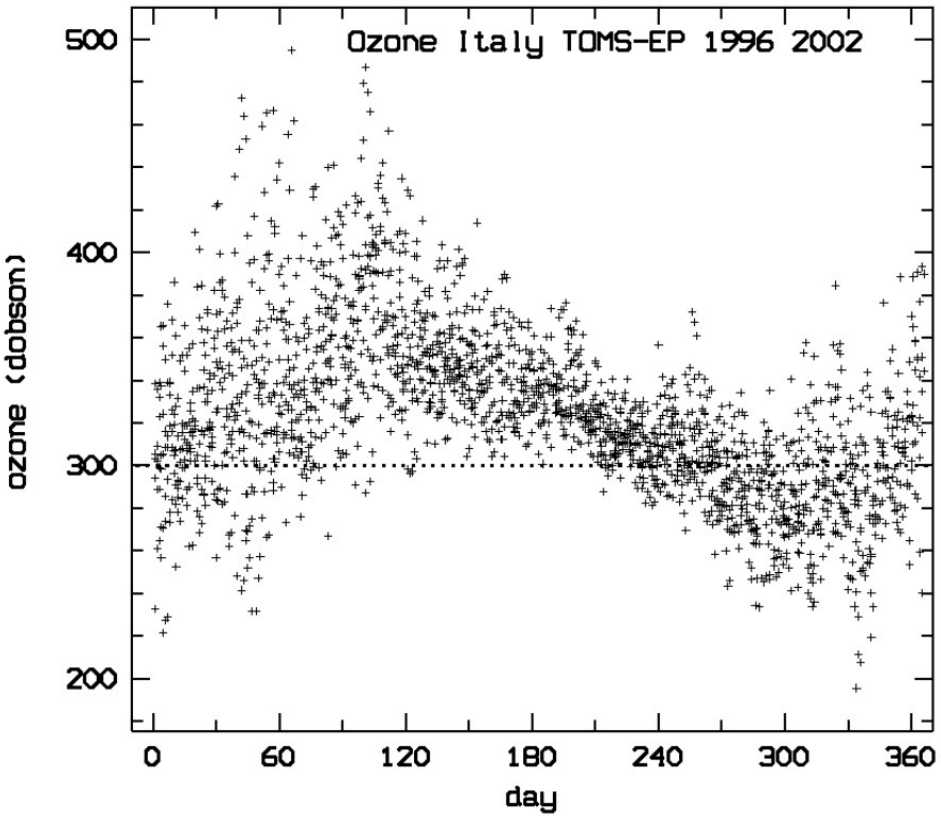

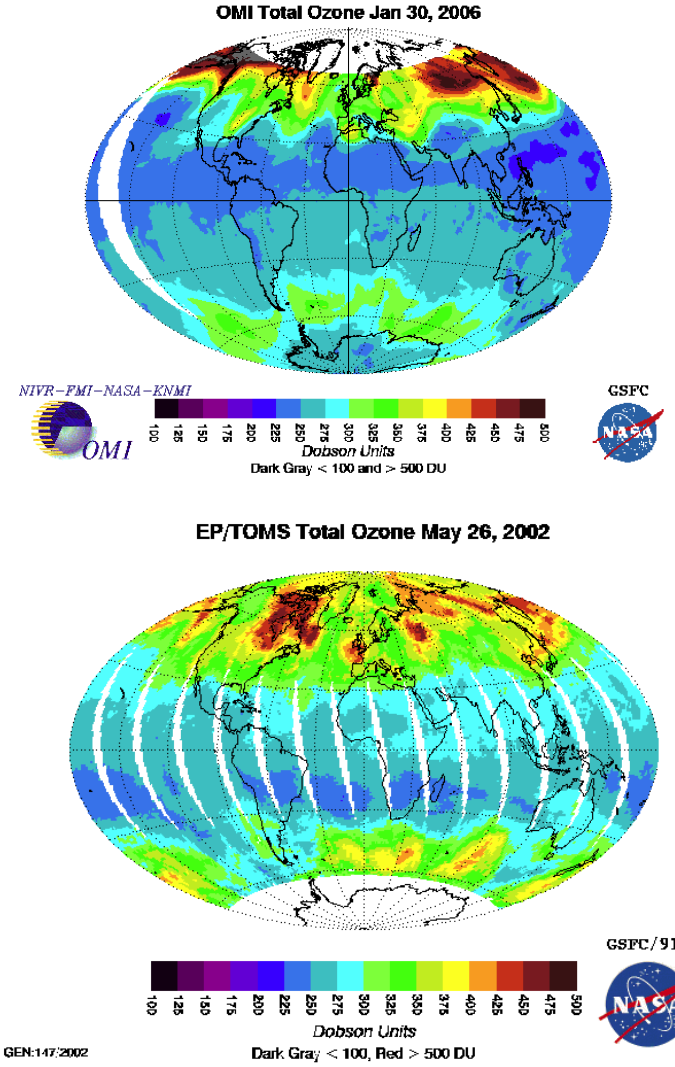

Ozono troposferico, calcolato dai residui di assorbimento totale – ozono stratosferico (1979 - 2000): in Italia picco estivo.
V. plot della concentrazione locale in Veneto (da ARPAV)
Totale troposferico circa 33 +/- 10 DB

http://asd-www.larc.nasa.gov/TOR/images/seasonal/global/TOR.Seasonal.Global.CLIM.jpeg

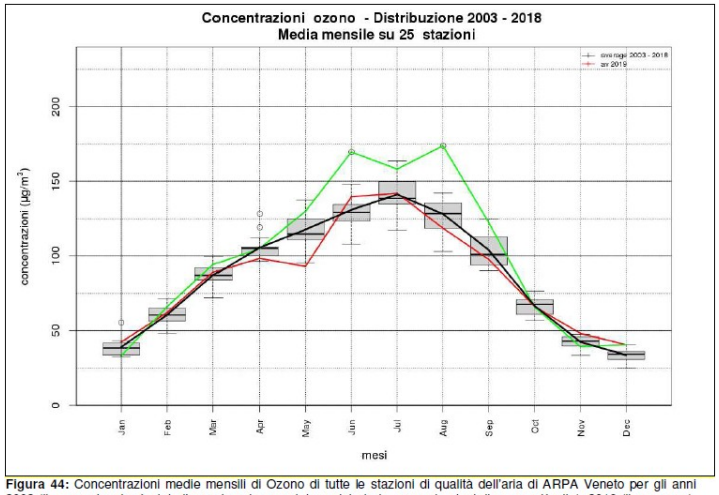

Figura 44: Concentrazioni medie mensili di Ozono di tutte le stazioni di qualità dell'aria di ARPA Veneto per gli anni 2003 (linea verde, che è stato l'anno in cui sono state registrate le concentrazioni di ozono più alte), 2019 (linea rossa), media anni 2003-2018 (linea nera). L'andamento medio mensile degli anni dal 2003 al 2018 è rappresentato anche mediante box and whiskers plot. (Per l'interpretazione del box and whiskers plot fare riferimento al riquadro Tabella 9 Come interpretare il box and whiskers).

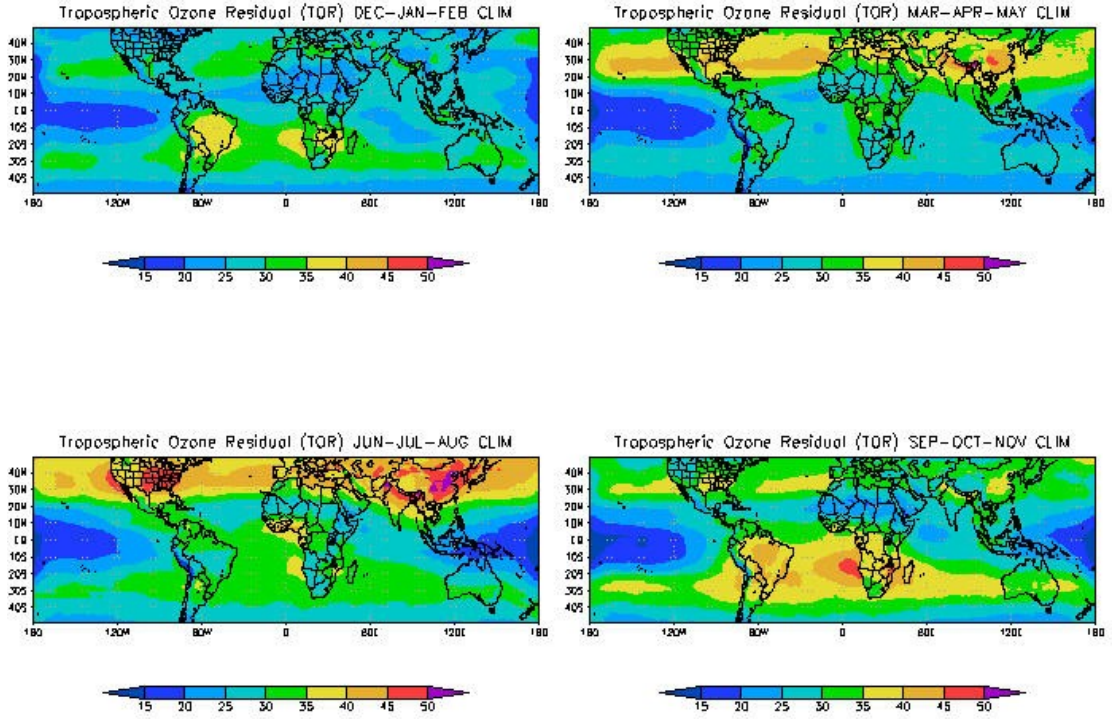

Mappe ozono stratosferico TOMS (Environment STB Canada)

e modelli-misure meteo (Vittori O.)

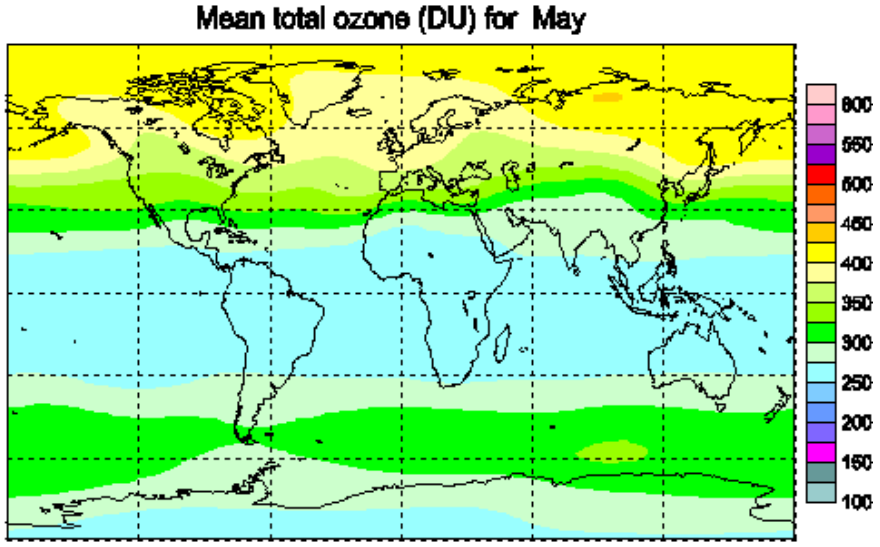

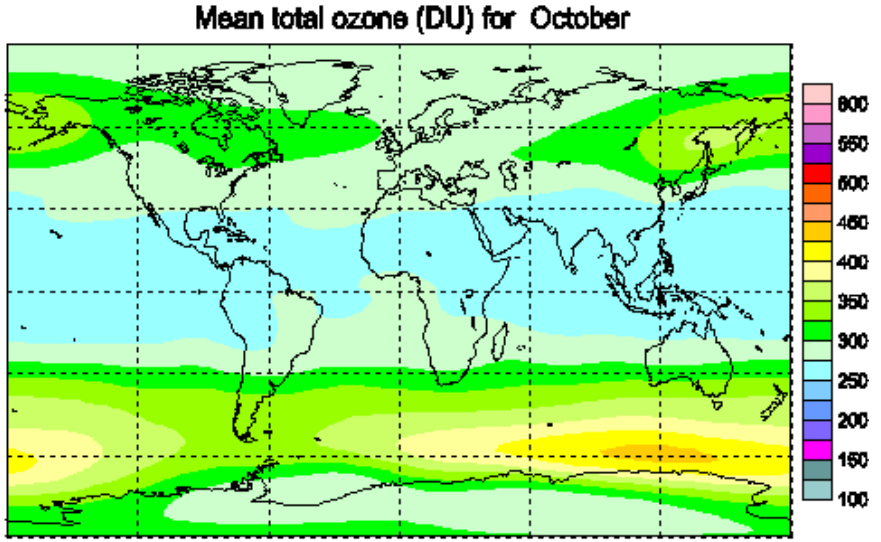

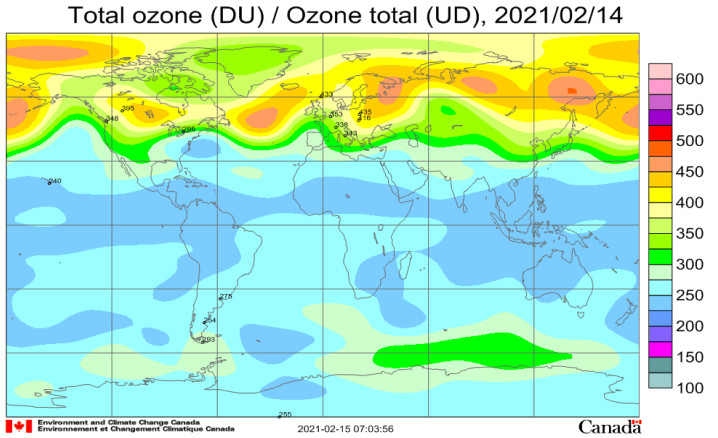

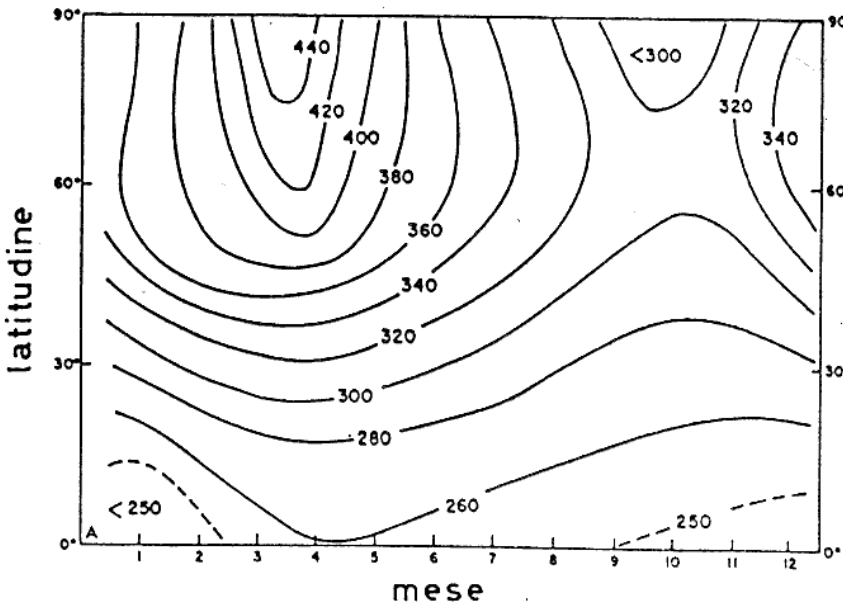

Figura 10. *Isolinee di spessore ottico di ozono espresso in dobson in funzione della latitudine e della stagione. I numeri in ascissa indicano gli inizi dei mesi dell'anno.*

ELT Site UV ESO Report (Ortolani and Gilmozzi)

$$I = I_0 \, e^{-K \, m(O3)}$$

I is the transmitted intensity, I_0 the radiation at the top of the atmosphere, K the absorption coefficient of the ozone and m(O3) the ozone atmospheric thickness (on average 0.3 cm in the reference standard atmosphere). The coefficient K has can be obtained from the literature (Vigroux, 1967, Bass and Paur 1984 or Bird and Riordan, 1984 for on line data). There is a wide literature on the discussion of the K variations with temperature and pressure. Typical values are around 2.5 at 310 nm and 10 at 300 nm.

The corresponding optical thickness (τ = 0.3 x K for standard ozone content) at 310 nm is about 0.3 and it increases above 3 at 300 nm, and around 36 at 280 nm
In a first approximation, a reduction of the ozone thickness from 300 to 200 Dobson units corresponds to a transmission increase by a factor 5 at 300 nm (from 1% to 5%) and by two orders of magnitudes at 290 nm (from 5×10^{-3} % to 4×10^{-1} %)

TABLE 1: calculated values of the optical depth due to Raileigh scattering at the sea level, at 4200m height, ozone optical depth, total optical depth, transmission (TR), transmission measured at Mauna Kea, transmission calculated at 4200m, transmission calculated at 4200m with 270 Dobson

Wavelength nm	**τ_R**	**τ_R(4200m)**	**KO_3**	**τO_3**	**τ_{tot}**	**TR (%)**	**TR (MK)**	**TR (4200m)**	**TR(4200m,270D)**
330	**.72**	**.43**	**0.09**	**0.03**	**0.75**	**47%**	**59%**	**59%**	**59%**
310	**.93**	**.56**	**2.5**	**0.75**	**1.68**	**19%**	**29%**	**27%**	**29%**
308	**.95**	**.57**	**3.45**	**1.03**	**1.99**	**14%**	**24%**	**20%**	**22%**
300	**1.06**	**.64**	**10.6**	**3.18**	**4.2**	**1.5%**	**-**	**2.2%**	**2.9%**
290	**1.21**	**0.72**	**29.0**	**8.7**	**9.9**	**5x10-3%**	**-**	**5x10-3%**	**0.02%**
280	**1.4**	**0.84**	**120**	**36**	**37.4**	**6x10-15%**	**-**	**-**	**2x10-13%**

Numero giorni piovosi in Italia come proxy per la copertura nuvolosa media mensile (da Bernacca, 1971)

Numero *medio* di giorni con pioggia (mesi)

Località	*G*	*F*	*M*	*A*	*M*	*G*	*L*	*A*	*S*	*O*	*N*	*D*
Alghero	10	7	6	6	4	2	1	1	4	7	7	11
Ancona	9	8	9	9	9	8	4	5	7	11	10	9
Aosta	5	4	6	6	7	6	6	6	6	7	7	6
Bari	12	11	10	11	8	5	3	4	6	10	11	13
Bologna	8	8	10	11	12	9	5	6	8	12	10	10
Bolzano	4	3	6	7	10	9	8	8	8	7	7	5
Cagliari	9	9	11	10	7	5	1	1	4	8	11	12
Catania	8	7	6	6	4	1	1	1	4	6	8	9
Enna	10	6	5	4	5	2	1	2	4	8	6	7
Firenze	9	9	11	12	11	10	5	5	8	13	12	12
Foggia	8	7	7	9	7	6	2	4	5	7	7	8
Genova	9	9	11	12	12	9	6	6	9	13	12	11
Livorno	10	9	11	10	9	6	3	4	7	13	12	12
Milano	9	8	10	12	13	11	8	8	8	12	11	10
Napoli	12	11	12	12	9	6	3	3	7	12	13	14
Padova	7	7	6	6	10	8	9	6	8	8	7	8
Palermo	15	13	12	7	6	4	2	2	6	12	13	16
Perugia	10	9	12	13	13	11	6	5	9	13	12	11
Pescara	8	6	6	6	6	4	3	4	7	9	8	7
Potenza	9	9	10	12	9	7	4	5	7	11	10	12
Roma	11	9	11	12	9	6	2	3	6	12	13	12
S. Remo	5	6	6	6	6	4	2	2	4	8	7	5
Sassari	12	10	11	10	8	5	1	2	6	12	14	14
Siena	8	7	9	10	10	8	4	4	7	11	10	9
Sondrio	6	6	7	8	12	13	10	9	10	10	7	5
Torino	7	6	8	13	14	13	9	8	9	10	9	7
Trento	4	5	6	8	12	10	8	8	8	7	8	6
Trieste	7	7	7	8	10	9	8	6	7	10	9	9
Venezia	6	6	9	9	11	10	7	6	7	10	9	8

Calcolo **stagionalità** UVB a Milano e Catania
febbraio-luglio
(declinazione Sole -14 a febbraio, +22 a luglio)

Milano: dz Sole dallo zenit 23 gradi in luglio, 61 in febbraio, con **5 mag./airmass**, corretto per nuvolosità (1.0) e ozono 30% (minimo !) -> R=112

Catania: dz Sole dallo zenit 16 gradi in luglio, 53 in febbraio, corr. per nuvolosità (1.26) e ozono → R=22

La variazione in funzione della massa d'aria domina largamente la stagionalità che è molto maggiore a nord

Airmass = cosec function

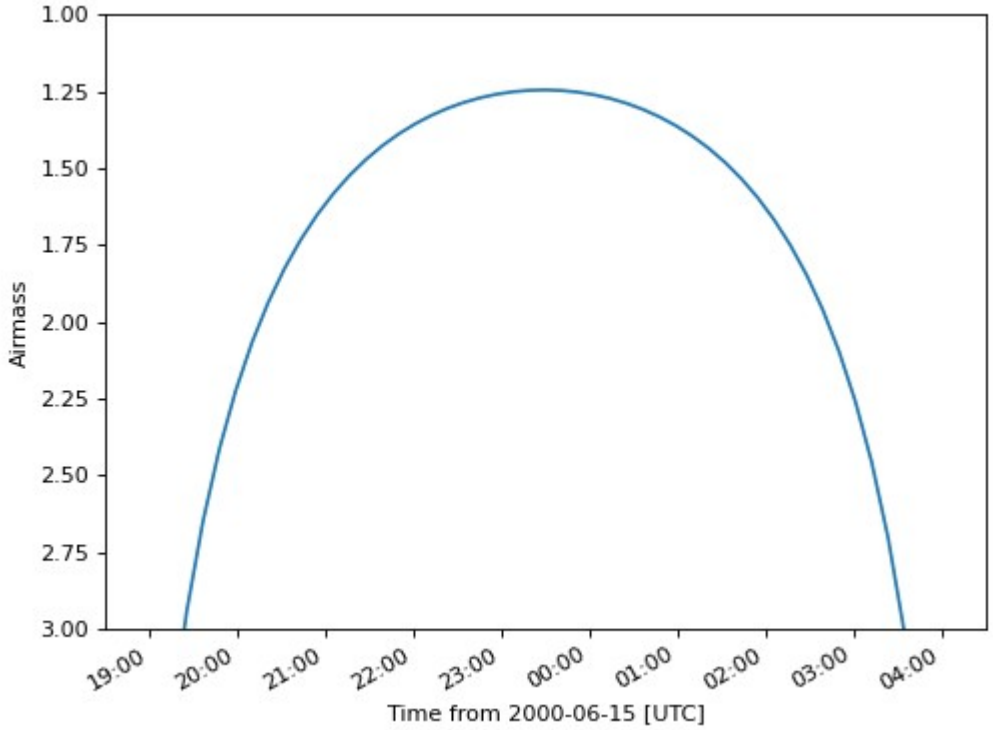

Radiazione UV-B vs. attività solare da INPE S. Space Obs. (400m): anticorrelati

Rampelotto et al., 2009, AIP conf.

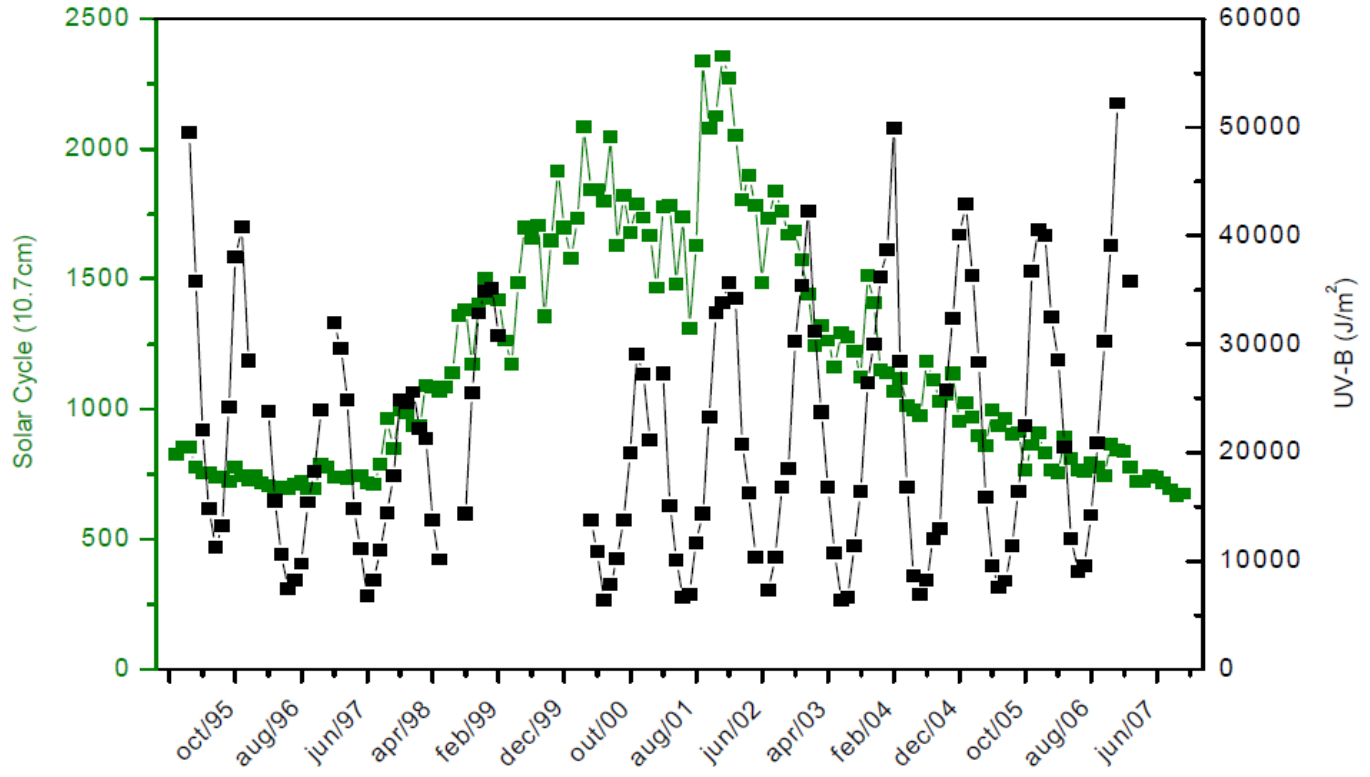

FIGURE 1: Monthly solar activity (left y axis, green point/line) and UV-B (right y axis, black point/line) measured at the INPE's Southern Space Observatory (29°S, 53°W) from 1995 to 2007.